

# Enhanced Crack Segmentation Algorithm Using 3D Pavement Data

Chenglong Jiang<sup>1</sup> and Yichang James Tsai<sup>2</sup>

**Abstract:** Automatic pavement crack segmentation has gained attention among researchers and transportation agencies over the past two decades. However, most existing algorithms using two-dimensional (2D) pavement intensity images cannot provide a satisfactory performance. With the advent of sensing technology, three-dimensional (3D) line laser pavement imaging systems have become available. The objective of this paper is to propose an enhanced dynamic optimization algorithm employing the advantages of 3D pavement data to improve crack segmentation. The proposed algorithm consists of three major stages. First, a two-step Gaussian filter is applied to remove outliers from the collected laser data and rectify the profile in order to reduce the influence of cross-slope and ruts on crack segmentation. Then, a rough crack segmentation stage is conducted to adaptively identify the crack regions of interest. Finally, a bounding box and major orientation for each valid crack region of interest will provide searching space and direction for the precise crack segmentation using the dynamic optimization algorithm. Experimental tests were conducted using actual pavement data collected near Savannah, Georgia. The four most common types of pavement cracking (longitudinal, transverse, block, and alligator cracking), as well as distress-free pavements, are tested, and the performance between original dynamic optimization algorithm and the proposed algorithm is compared. Experimental results show that the proposed algorithm takes only about 1/4 of the average computation time of the original algorithm. Also, the accuracy of crack segmentation has been improved since the proposed algorithm removes the unnecessary false positives and handles cracks in multiple directions better. Finally, conclusions are drawn, and recommendations for future research are discussed. DOI: [10.1061/\(ASCE\)CP.1943-5487.0000526](https://doi.org/10.1061/(ASCE)CP.1943-5487.0000526).

© 2015 American Society of Civil Engineers.

**Author keywords:** Crack segmentation; Three-dimensional (3D) pavement data; Dynamic optimization.

## Introduction

Pavement surface distress evaluation is an essential component of a pavement management system (PMS). One of the most common types of pavement distresses is cracking. Pavement cracking is caused by constant overloading, pavement aging, environmental impacts, improper structural design, and other factors. The proper treatment of pavement cracks at the optimal time is important for a cost-effective pavement maintenance strategy. A total of 94 percent of all state departments of transportation (DOTs) monitor cracking data for the National Highway System (NHS) ([Federal Highway Administration 2015](#)). Visual surveys conducted by engineers in the field are still the most widely used means to inspect and evaluate pavements, although such evaluations involve high degrees of subjectivity, hazardous exposure, and low production rates ([Goodman 2001](#)). Consequently, automated crack segmentation and classification are gaining wide popularity among transportation agencies.

As early as 1990, Haas and Hendrickson ([1990](#)) presented a general model of pavement surface characteristics that integrated multiple types of sensor information to simplify the process of

automated pavement distress surveying. Wang ([2000](#)) and Wang and Gong ([2002](#)) introduced an automated system capable of collecting and analyzing pavement surface distresses (primarily cracks) in real time through the use of digital cameras; similar intensity imaging setups have also been used by many other researchers. Ahmed and Haas ([2010](#)) used a low-cost photogrammetric system to reconstruct a three-dimensional (3D) model of a pavement surface. Jahanshahi et al. ([2013](#)) used a RGB-D sensor, which collects additional depth information with an infrared projector, to detect and quantify pavement defects. Laurent et al. ([2008](#)) introduced a high-resolution laser imaging system to collect 3D pavement data. Many state DOTs, also have made efforts to automate the taking of pavement condition surveys. The Texas DOT ([Xu 2005, 2007](#)) used artificial lighting as the ultimate solution for eliminating all shadows in an image and for improving data uniformity across different weather conditions. The Florida DOT ([Mraz et al. 2006, 2007](#)) conducted a comprehensive evaluation of pavement distress systems by looking into different factors, including spatial resolution, brightness resolution, optical distortion, and signal-to-noise ratio, and developed a multipurpose survey vehicle, including related automatic applications. The Ministry of Transportation of Ontario ([Capurucu et al. 2006; Tighe et al. 2008](#)) conducted a performance evaluation of current technologies for taking automated pavement condition surveys.

Two-dimensional (2D) pavement intensity images are used in most automatic crack segmentation methods. Cheng ([1999](#)) proposed an automatic crack segmentation and classification method based on fuzzy set theory. Lee and Lee ([2004](#)) provided a neural-network-based approach for automatic crack analysis based on digital pavement images. Zhou et al. ([2005, 2006](#)) decomposed a pavement image into different frequency subbands by wavelet transform and identified cracks through statistical criteria from

<sup>1</sup>Graduate Student, School of Civil and Environmental Engineering, Georgia Institute of Technology, 790 Atlantic Dr. NW, Atlanta, GA 30332-0355. E-mail: [clijiang@gatech.edu](mailto:clijiang@gatech.edu)

<sup>2</sup>Professor, School of Civil and Environmental Engineering, Georgia Institute of Technology, 790 Atlantic Dr. NW, Atlanta, GA 30332-0355 (corresponding author). E-mail: [james.tsai@ce.gatech.edu](mailto:james.tsai@ce.gatech.edu)

Note. This manuscript was submitted on February 25, 2015; approved on July 9, 2015; published online on August 31, 2015. Discussion period open until January 31, 2016; separate discussions must be submitted for individual papers. This paper is part of the *Journal of Computing in Civil Engineering*, © ASCE, ISSN 0887-3801/04015050(\$25.00).

high-amplitude wavelet components. Adu-Gyamfi et al. (2012) used the empirical mode decomposition method to reduce the impact of different illumination effects on defect detection. Most of these existing crack segmentation algorithms use a local-based image processing method, as the segmentation of crack pixels relies completely on the local information in a small neighborhood. Although generally, cracks bear elevations that are lower than the surrounding pavement, the contrast of cracks may be seriously weakened by background noises, such as pavement surface texture and raveling, possible crack degradations, such as the width and depth change along the cracks, and foreign debris inside the cracks. As a result, local-based crack segmentation algorithms usually detect a set of disconnected crack fragments with many false positives (Zou et al. 2012). Compared to these local-based algorithms, the dynamic optimization-based crack segmentation algorithm (Alekseychuk 2006), designated as *dynamic optimization algorithm* hereafter in this paper, has demonstrated an outstanding performance in terms of segmentation accuracy, since it calculates the likelihood of the presence of a crack indication at a pixel instead of a single yes/no decision. Evaluated by a buffered Hausdorff distance-based scoring measurement, which is also used for accuracy evaluation in this study, the dynamic optimization algorithm outperforms five other existing algorithms, including statistical thresholding, Canny edge detection, a multiscale wavelet method, a crack seed identification method, and an iterative clipping method (Tsai et al. 2010). However, the computation time limits its practical implementation with automated crack surveys.

With the advances of sensing technology, high-resolution 3D line laser imaging systems are now available. In 3D pavement data, pavement cracking becomes more distinctive, with its apparent elevation change, and the influences of most noises on 2D intensity images have been reduced. Since almost all the existing methods focus on 2D intensity images, there is a need to develop an automatic algorithm to better utilize the advantage of 3D pavement data on crack segmentation. The objective of this paper is to propose an enhanced algorithm to achieve fast and accurate crack segmentation using 3D pavement data. The paper is organized as follows. The second section presents an overview of the original dynamic optimization algorithm. The third and fourth sections present the proposed enhanced algorithm and experimental results. The last section concludes the paper and recommends future research directions.

## Dynamic Optimization-Based Crack Segmentation

In this section, a brief overview of dynamic optimization-based crack segmentation is presented. Alekseychuk (2006) developed the dynamic optimization algorithm for detecting cracklike indications in digital radiography and medical imaging. In general, it utilizes an approach of the detection of local discontinuities, followed by a grouping algorithm.

### Detection of Local Discontinuities

First, a local operator is developed, which calculates the likelihood of the presence of an indication of the given intensity in the given image point. Instead of directly detecting a local discontinuity with a single yes/no decision, such an operator provides an abstraction of the physical image, which prevents the loss of information and is suitable for cracklike defect detection under a low signal-to-noise ratio (SNR) environment. To estimate the indication intensity  $z(x)$ , a profile of an indication of width  $w_{\text{ind}}$  located on a changing background around the point  $x$  is used (as shown in Fig. 1). On this profile, two areas are used for background estimation, each of

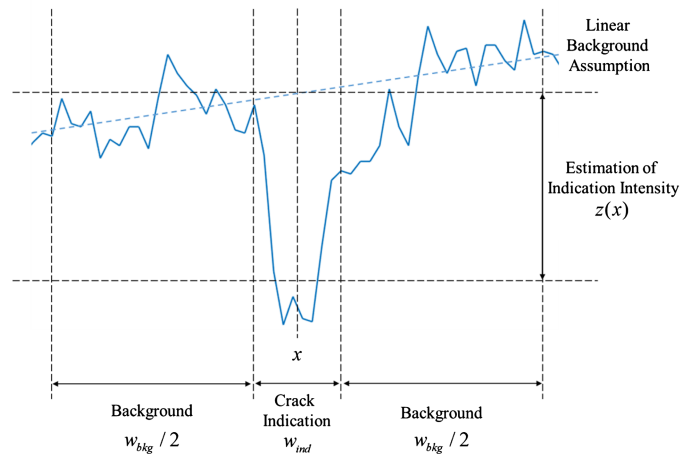


**Fig. 1.** Estimation of intensity of a crack indication (adapted from Alekseychuk 2006)

width  $w_{\text{bkg}}/2$  and symmetrically located on opposite sides of the crack indication. With a linear assumption of the changing background intensity, the background gray value at the center point  $x$  can be calculated with the least squares method as

$$g_{\text{bkg}}(x) = \frac{\sum_i g(i)}{w_{\text{bkg}}}, \\ i \in \left[ x - \frac{w_{\text{ind}}}{2} - \frac{w_{\text{bkg}}}{2}, x - \frac{w_{\text{ind}}}{2} \right] \cup \left[ x + \frac{w_{\text{ind}}}{2}, x + \frac{w_{\text{ind}}}{2} + \frac{w_{\text{bkg}}}{2} \right]$$

where  $g(i)$  equals the real pixel intensity at the point  $i$ . Similarly, the indication gray value at the center point  $x$  can be calculated as

$$g_{\text{ind}}(x) = \frac{\sum_j g(j)}{w_{\text{ind}}}, \quad j \in \left[ x - \frac{w_{\text{ind}}}{2}, x + \frac{w_{\text{ind}}}{2} \right]$$

The estimation of the indication intensity  $z$  is the difference between the background gray value and the indication gray value

$$z(x) = g_{\text{bkg}}(x) - g_{\text{ind}}(x) = \frac{\sum_i g(i)}{w_{\text{bkg}}} - \frac{\sum_j g(j)}{w_{\text{ind}}} \\ i \in \left[ x - \frac{w_{\text{ind}}}{2} - \frac{w_{\text{bkg}}}{2}, x - \frac{w_{\text{ind}}}{2} \right] \cup \left[ x + \frac{w_{\text{ind}}}{2}, x + \frac{w_{\text{ind}}}{2} + \frac{w_{\text{bkg}}}{2} \right] \\ j \in \left[ x - \frac{w_{\text{ind}}}{2}, x + \frac{w_{\text{ind}}}{2} \right]$$

Assuming that the noise at each pixel is under Gaussian distribution with a zero mean and a standard variance  $\sigma$ , the standard deviation of this estimation is

$$\sigma_z = \sqrt{\left(\frac{\sigma}{w_{\text{bkg}}}\right)^2 + \left(\frac{\sigma}{w_{\text{ind}}}\right)^2} = \sigma \sqrt{\frac{w_{\text{bkg}} + w_{\text{ind}}}{w_{\text{bkg}} w_{\text{ind}}}}$$

However,  $z$  is the observed random variable as a combination of the true indication intensity  $h$  and the random noise component  $\nu$ . For a scenario with noise ( $\nu \neq 0$ ), the estimation of  $z$  alone is insufficient to describe a crack indication since indications of different intensities  $h$  may result in the same  $z$  due to noise influence, and vice versa. Under this scenario, the crack indication can be characterized by a posteriori distribution  $\rho(h|z)$ , which is the probability distribution of crack indication with intensity  $h$  given estimation  $z$ . According to the Bayesian rule,

$$\rho(h|z) = \frac{\rho(h)\rho(z|h)}{\rho(z)}$$

where the likelihood  $\rho(z|h)$  can be modeled as the Gaussian distribution of argument  $z$  with mean  $h$  and standard deviation  $\sigma_z$ . That is

$$\rho(z|h) = \frac{1}{\sqrt{2\pi\sigma_z^2}} e^{-(h-z)^2/2\sigma_z^2}$$

It is further assumed that the indication of the known intensity  $h$  can be present with a priori probability  $P(h)$  or absent with a priori probability  $[1 - P(h)]$ . The values  $P(h)$  and  $h$  must be externally provided to the algorithm as parameters. This simplifies the calculation of the a posteriori probabilities into two possible cases of indication presence  $P(h|z)$  and absence  $P(0|z)$ , as well as the subsequent comparison between them.

### Global Optimization of Crack Indications

Then, the local estimations serve as an input for a grouping algorithm, under the assumption that a global feature (i.e., an estimation function) calculated on a set of consecutive points along the full indication length will be less influenced by the noise than will a single local estimation. Let  $P_1$  and  $P_0$  denote the probabilities of hypotheses of indication presence and absence, respectively, and the joint a posteriori probabilities of both hypotheses for a path can be represented through local probabilities in each point of the path:

$$P_1(p_1, p_2, \dots, p_n) = P_1(p_1)P_1(p_2), \dots, P_1(p_n)$$

$$P_0(p_1, p_2, \dots, p_n) = 1 - P_1(p_1, p_2, \dots, p_n)$$

where  $P_1(p_i)$  is the a posteriori probability of indication presence at the point  $p_i$ , which can be calculated as

$$P_1(p_i) = \frac{P(h)\rho[z(p_i)|h]}{\rho[z(p_i)]}$$

$$\rho[z(p_i)] = P(h)\rho[z(p_i)|h] + [1 - P(h)]\rho[z(p_i)|0]$$

Then, global optimization with dynamic programming is conducted to find the optimal path of crack pixels at the defined probability function.

### Application to a Crack Segment with 3D Pavement Data

The original dynamic optimization algorithm is applied on 3D data, as shown in Fig. 2. The following can be observed:

1. The dynamic optimization algorithm can also be applied to 3D pavement data. One key assumption of this algorithm is that the crack pixel has a lower intensity value than its surrounding area. For 3D data, it represents the elevation change instead of the intensity change on the pavement, where pavement cracking usually has a low elevation. Therefore, when converting the 3D pavement data into a range image, each pixel represents the relative elevation of that point, and the crack pixel still has a lower value compared to its neighborhood. The left image shown in Fig. 2 is the range image of 3D pavement data, and the right image shows the crack segmentation results using the dynamic optimization algorithm. The longitudinal crack on the left of the image is well preserved through the segmentation.

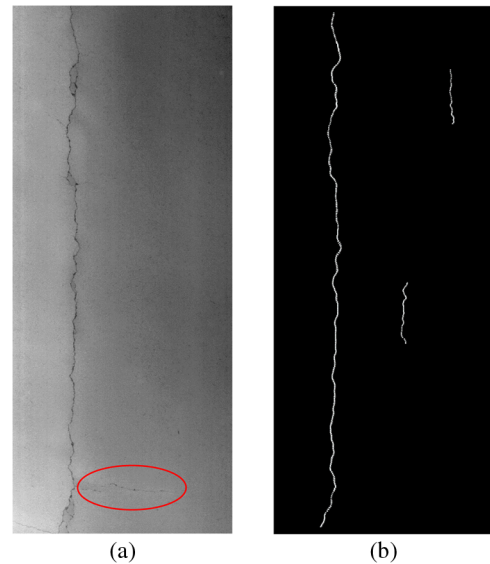


**Fig. 2.** Crack segment using 3D pavement data: (a) range image; (b) crack segmentation results using dynamic optimization

2. The dynamic optimization algorithm is sometimes overly sensitive to background noises on the image. This will lead to a certain number of false positive segmentation results. In Fig. 2(b), the segmented short curves on the right are actually not crack lines. However, due to tiny elevation changes in those areas, they are still captured by the algorithm as false positives.
3. Since the dynamic optimization algorithm basically defines the probability of a crack indication from one-dimensional (1D) perspective, it requires an input as a default “searching direction.” This means that the algorithm will focus more on the crack segmentation in the given direction. Although it still has a certain tolerance and robustness when handling the meandering crack curves, it doesn’t perform quite as well when cracks in multiple directions appear in the same searching area. As shown in Fig. 2, the transverse crack on the bottom (highlighted by the red circle) was not correctly segmented.
4. The default search space of dynamic optimization crack segmentation is the entire image. When the resolution of data increases, the computation time increases exponentially. This problem is more notable when dealing with 3D pavement data, most of which are of a high resolution. This issue may impede the implementation of real applications. Huang and Tsai (2011) introduced the region of interest (ROI) as a search space instead of the entire image. However, the ROI setting was based on fixed image tiles and is not quite flexible. Also, although the computation time was reduced, their solution still didn’t deal with the limitations mentioned here.

### Proposed Methodology

In order to improve the performance of crack segmentation on 3D pavement data, the enhanced dynamic optimization-based crack segmentation method is presented in this section. The proposed method consists of the following steps:

1. Outlier removal and profile rectification;
2. Rough segmentation through local thresholding and connected component analysis; and

3. Precise segmentation using the dynamic optimization algorithm.

The following subsections will explain each step in detail.

### Outlier Removal and Profile Rectification

Crack segmentation using a traditional 2D intensity image suffers from different lighting conditions, low contrast, and other pavement surface objects, such as pavement markings and oil stains. Comparatively, 3D pavement data has an advantage when dealing with those situations. However, 3D pavement data also has noise sources. Two major noise sources when using 3D pavement data on crack segmentation are

- Invalid laser points and outliers: A 3D line laser pavement imaging system needs to capture the information of each laser point that it sent out previously. Considering the high scanning frequency, invalid laser points and outliers happen more than in traditional 2D photos. These points usually appear to have a sharp elevation changes compared to their surrounding area and will have certain influences on crack segmentation.
- Pavement features involving elevation changes: At lower frequency bands, the pavement itself has certain features involving elevation changes, including cross-slope and rut. Effective removal of these features from the pavement profiles will help enhance the detection of the presence of pavement cracking and improve the performance of crack segmentation.

Therefore, the first stage of the proposed method is outlier removal and profile rectification. A two-step profile rectification process is presented here using a Gaussian filter. The typical 1D Gaussian filter with the standard deviation  $\sigma$  is

$$g(x) = \frac{1}{\sqrt{2\pi}\sigma} e^{-(x^2/2\sigma^2)}$$

The function of the Gaussian filter depends on the value of  $\sigma$ . The first step is to remove the invalid points and outliers from the raw data. Therefore, a Gaussian filter with a small value of  $\sigma$  (in this case,  $\sigma = 8$ ) is chosen to check if each point on the profile has an unusual sharp elevation change compared to its closest neighborhood; i.e.,

$$\text{Range}'(x) = \begin{cases} \text{Range}(x) & \text{if } \text{abs}[\text{Range}(x) - \text{FRange}(x)] > \text{thres} \\ \text{FRange}(x) & \text{otherwise} \end{cases}$$

where  $\text{Range}(x)$  is the original profile at point  $x$ ,  $\text{FRange}(x)$  is the filtered profile at point  $x$ , and  $\text{thres}$  is a given threshold.

After the outlier removal, another Gaussian filter with a much larger  $\sigma$  (in this case,  $\sigma = 150$ ) is applied to smooth the entire profile and identify the cross-slope and rutting. Let  $\text{FRange}'(x)$  be the filtered profile based on  $\text{Range}'(x)$ ; then the rectified profile will be

$$\text{RecRange}(x) = \text{FRange}'(x) - \text{Range}'(x)$$

Fig. 3 shows an example of profile rectification on one transverse profile. The image on the top is the original pavement profile, and the red line is the smoothed profile. The rectified profile on the bottom is then generated by the subtraction of the smoothed profile and the original profile. Fig. 4 shows the profile rectification results for the entire image. It can be observed that after this stage, the elevation of the entire range image has been adjusted and crack features have been enhanced. It needs to be noted that the Gaussian filter can be applied in both one dimension and two dimensions. In this case, considering the fact that the 3D pavement data are collected through a line laser imaging system, only a 1D Gaussian

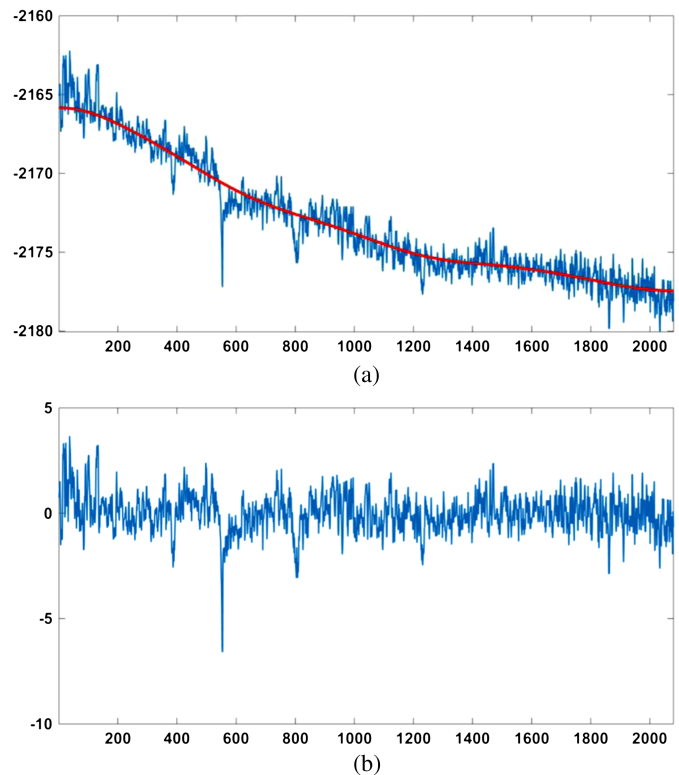


**Fig. 3.** Example of profile rectification on one transverse profile: (a) original profile; (b) rectified profile

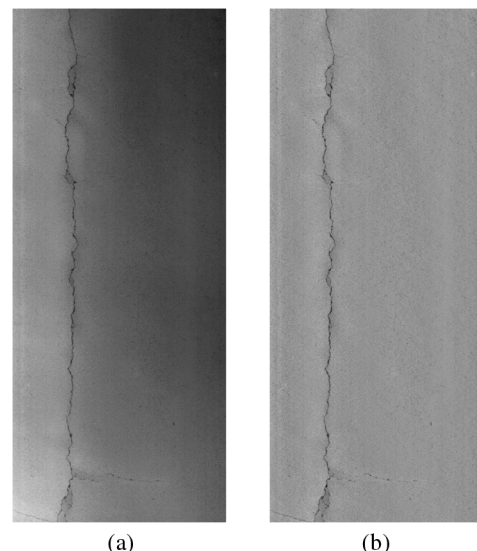


**Fig. 4.** Results of profile rectification on the entire range image: (a) original range image; (b) rectified range image

filter is applied; i.e., each transverse profile is rectified separately and then combined into a rectified range image.

### Rough Segmentation through Connected Component Analysis

Based on the rectified range image, a rough segmentation is proposed in order to adaptively determine the crack ROIs and the input

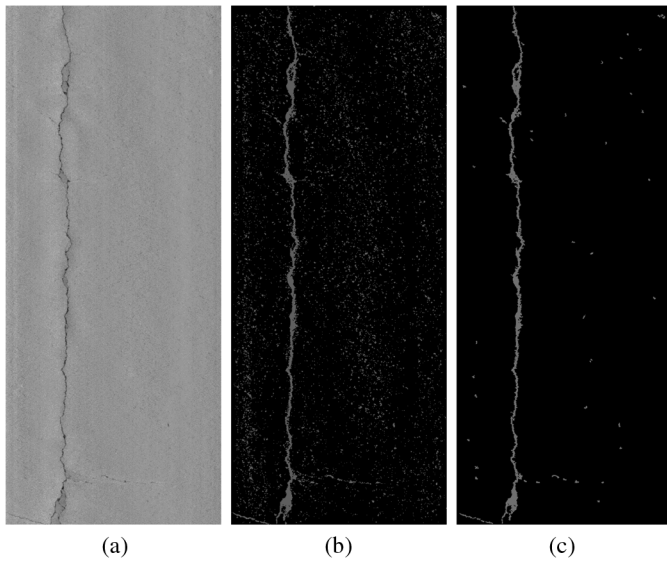
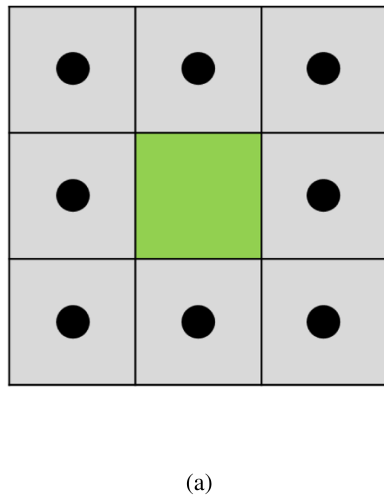


**Fig. 5.** Illustration of rough crack segmentation: (a) rectified range image; (b) results of local thresholding; (c) results after connected component analysis

for the dynamic optimization algorithm. First, a local thresholding process is conducted to determine initial cracklike pixels by comparing their range values to their surrounding areas. Fig. 5(b) shows the results after thresholding. As expected, although the real crack pixels have mostly been preserved, many false positives can be observed.

Therefore, a connected component analysis is conducted to further refine the initial segmentation, which is a process to uniquely label subsets of connected components based on a given connectivity heuristic. An eight-connectivity heuristic is used in this study. Fig. 6(a) shows an image region of 3 pixels by 3 pixels; with the eight-connectivity heuristic, the green pixel in the center is connected to eight surrounding pixels. If one initial cracklike pixel from the thresholding process is connected to another, they are labeled as the same connected component. For each labeled connected component, the following properties are computed, as shown in Fig. 6(b). Some properties are similar to the ones previously used in a crack classification study (i.e., Tsai et al. 2014):



(a)

### Area

$A$  is defined as the number of cracklike pixels in the connected component. It will be used as a criterion to distinguish a valid connected component.

### Major Axis

$L$  is defined as the length of the major axis of the ellipse that has the same normalized second central moments as the group of  $N$  cracklike pixels  $(x_i, y_i)$  in a connected component:

$$L = 2 \times \sqrt{2[(\mu_{xx} + \mu_{yy}) + \Delta]}$$

where  $\mu_{xx} = \sum_{i=1}^N x_i^2/N$ ,  $\mu_{yy} = \sum_{i=1}^N y_i^2/N$ ,  $\mu_{xy} = \sum_{i=1}^N x_i y_i/N$ , and  $\Delta = \sqrt{(\mu_{xx} - \mu_{yy})^2 + 4 \times \mu_{xy}^2}$  are the second moments of the cracklike pixels in that connected component.

### Minor Axis

Similarly,  $S$  is defined as the length of the minor axis of the ellipse that has the same normalized second central moments as the group of cracklike pixels in a connected component:

$$S = 2 \times \sqrt{2[(\mu_{xx} + \mu_{yy}) - \Delta]}$$

### Bounding Box

The position and size ( $W$  and  $H$ ) of the bounding box are the inputs that will be provided to the following precise crack segmentation.

### Orientation

$O$  is a measure of the connected component direction relative to the horizontal axis of the data sample. It will be used as the searching direction to improve the performance of dynamic optimization:

$$O = \begin{cases} \frac{180}{\pi} \times \tan^{-1} \left( \frac{\mu_{xx} + \mu_{yy} + \Delta}{2\mu_{xy}} \right), & \text{if } \mu_{xx} < \mu_{yy} \\ \frac{180}{\pi} \times \tan^{-1} \left( \frac{2\mu_{xy}}{\mu_{xx} + \mu_{yy} + \Delta} \right), & \text{if } \mu_{xx} \geq \mu_{yy} \end{cases}$$

After these properties are computed for all the connected components, certain criteria are considered to refine the initial segmentation results in order to identify the effective crack ROIs. In this

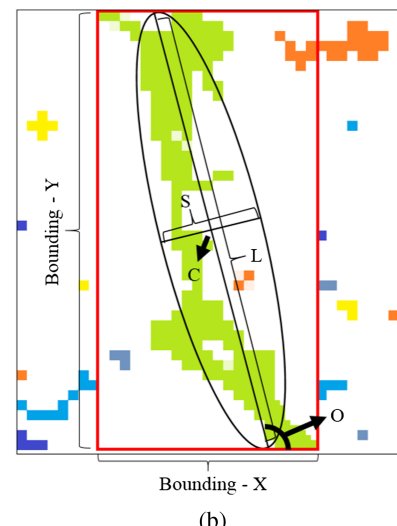


**Fig. 6.** Illustration of connected component analysis: (a) eight-connectivity; (b) properties of connected components (from Huang and Tsai 2011, Fig. 8, p. 95; copyright, National Academy of Sciences, Washington, DC; reproduced with permission of the Transportation Research Board)

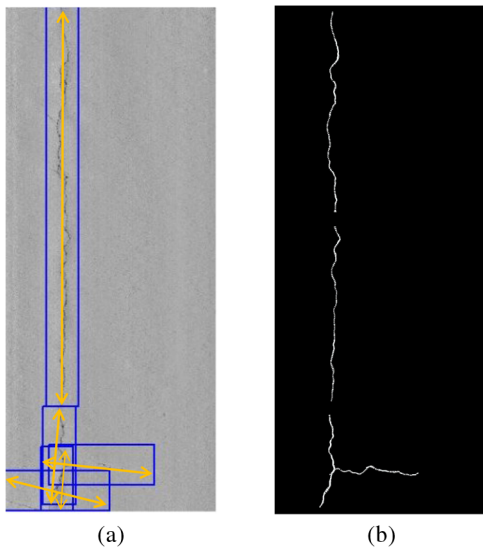


**Fig. 7.** Precise crack segmentation using the dynamic optimization algorithm: (a) adaptive crack ROIs and searching direction; (b) final segmentation results

study, two simple criteria were used: area and linear similarity. To be considered as a valid crack ROI, the connected component must have over 20 cracklike pixels, and since cracks are usually shaped as thin strips, the ratio of  $L$  to  $S$  must be greater than 1.5. These values

should vary corresponding to different data resolutions. After the connected component analysis, the false positives in initial segmentation results were significantly removed, as shown in Fig. 5(c).

### Precise Segmentation Using Dynamic Optimization

After the rough segmentation stage, each of the valid crack ROIs will generate an adaptive searching space for dynamic optimization algorithm. The inputs include two parts. The first part is the searching space, which is determined by the bounding box for each crack ROI. The dynamic optimization algorithm has a requirement of the minimum size of image region to run, with respect to areas used to calculate the background intensity on each profile. In addition, the crack segmentation becomes less robust when a crack appears to be close to the edge of the bounding box, as there is insufficient information on one side to estimate the crack indication. The bounding boxes of the valid connected components are extended with a small buffer in order to fulfill the minimal requirement of dynamic optimization and increase the robustness of crack segmentation, and the blue rectangles in Fig. 7(a) show the generated searching areas. In order to avoid confusion, not all the valid ROIs of this range image are displayed in Fig. 7.

The second part is the searching direction. The orientations of the valid connected components are used to constitute the searching direction for dynamic optimization, as shown by the orange arrows in Fig. 7(a). The dynamic optimization algorithm is executed on each of these searching spaces, and the results are combined as the final crack segmentation results [Fig. 7(b)].

**Table 1.** Performance of the Original Dynamic Optimization Algorithm and the Proposed Algorithm

Type	Number	Original algorithm		Proposed algorithm				Time—total (s)
		Accuracy (score)	Time—total (s)	Accuracy (score)	Time—profile rectification (s)	Time—rough segmentation (s)	Time—precise segmentation (s)	
Longitudinal	1	59.66	65.02	90.26	4.83	1.00	5.86	11.70
	2	51.99	233.07	85.54	5.93	1.72	14.00	21.66
	3	76.99	76.68	90.97	6.05	1.22	16.51	23.78
	4	68.73	123.37	90.25	5.50	1.22	9.12	15.83
	5	72.45	89.20	95.24	4.67	1.00	7.14	12.80
	Average	65.96	117.47	90.45	5.40	1.23	10.53	17.16
Transverse	6	0.00	50.22	96.26	3.93	0.85	10.30	15.08
	7	6.69	207.68	86.09	3.89	0.61	6.58	11.08
	8	0.02	231.00	80.64	4.19	0.64	5.56	10.39
	9	0.01	222.03	53.35	4.15	0.79	22.09	27.03
	10	11.64	224.03	92.97	4.74	0.94	5.68	11.36
	Average	3.67	186.99	81.86	4.18	0.77	10.04	14.99
Block	11	62.05	58.72	93.26	4.01	1.26	37.99	43.27
	12	35.66	153.98	80.27	4.30	1.02	15.87	21.19
	13	77.10	63.68	87.01	4.60	1.21	5.80	11.62
	14	74.09	52.46	92.60	4.50	1.12	12.34	17.96
	15	54.67	155.13	72.66	4.02	1.22	16.52	21.75
Alligator	Average	60.71	96.79	85.16	4.29	1.17	17.70	23.16
	16	76.10	213.83	90.77	5.04	1.13	99.78	105.94
	17	78.86	171.81	89.94	3.77	0.78	114.43	118.98
	18	74.69	176.84	91.40	3.63	0.78	112.34	116.75
	19	73.45	193.56	84.17	3.78	1.09	105.73	110.60
	20	73.33	194.14	72.02	3.70	0.73	57.47	61.90
None	Average	75.28	190.04	85.66	3.98	0.90	97.95	102.84
	21	100.00	15.50	100.00	3.81	1.75	0.12	5.69
	22	100.00	15.79	100.00	3.75	1.81	1.35	6.67
	23	100.00	15.14	100.00	3.78	1.12	0.60	5.50
	24	0.00	39.70	100.00	3.60	2.36	19.30	25.26
	25	100.00	15.34	100.00	3.89	2.21	14.27	20.37
Overall	Average	80.00	20.29	100.00	3.77	1.85	7.13	12.70
	Average	57.13	122.31	88.62	4.32	1.19	28.67	34.16

## Experimental Results

The objective of this experimental test was to demonstrate the performance of the proposed algorithm in terms of accuracy and time consumption. The data set used for this test included actual 3D pavement data collected on U.S. 80/Louisville Road near Savannah, Georgia, using the laser crack measurement system (LCMS) from the National Optics Institute (INO) (Laurent et al. 2008). This is a line laser imaging system based on the laser triangulation principle that collects transverse pavement profiles consecutively as the vehicle is being driven at a speed of 100 km/h. Each pavement image in this study covered an area of 5 m in the driving direction and about 2 m in the transverse direction. The resolution of all the range images was resized to  $1,250 \times 520$ . The data set covered the four most common types of pavement cracking (longitudinal, transverse, block, and alligator cracking), as well as distress-free pavement.

### Accuracy

To effectively assess the accuracy of the proposed algorithm, the buffered Hausdorff distance-based scoring measure was adopted, which has been demonstrated to be the best quantitative evaluation measure compared to four other measures for measuring the accuracy of crack segmentation algorithms (Kaul et al. 2009). The buffered Hausdorff distance is given by

$$BH(G, S) = \max[h(G, S), h(S, G)]$$

where

$$h(G, S) = \frac{1}{m} \sum_{a \in G} \text{sat} \min_L \min_{b \in S} \|a - b\|$$

Here,  $G$  and  $S$  are coordinate locations of the crack pixels in the ground truth image and the segmentation results, respectively;  $a$  and  $b$  are each crack pixel in the ground truth image and the segmentation results, respectively;  $m$  is an average factor equal to the number of crack pixels in  $G$ ; and  $\text{sat}$  indicates that when the distance of one crack pixel to the closest crack pixel in the other image exceeds a saturation value  $L$ , we use a constant value of  $L$  for the distance. The reason for introducing a saturation value is that once a crack pixel in the automatically segmented image falls substantially away from the closest pixel in the ground truth image, it no longer makes sense to heavily penalize this distance; wrong detections beyond a certain distance should be penalized equally. The quantitative score is then computed as

$$\text{Score} = 100 - \frac{BH(G, S)}{L}$$

The buffered Hausdorff score ranges from 0 to 100, where 100 indicates perfect crack segmentation. In order to conduct this quantitative evaluation, all the range images were manually digitized to establish the ground truth location of crack pixels. It is noted that at the current image resolution (i.e.,  $1,250 \times 520$ ), some fine cracks (e.g., around 2 mm wide) on the pavement became unobservable or partially observable on a range image. To achieve a fair comparison, the resized range image was used to establish the ground truth. The proposed algorithm was fully compatible with higher-resolution images to detect these fine cracks, but consequently, the time consumption became higher.

### Time Consumption

In terms of time consumption, the experimental test was conducted on a computer with Intel Core2 Duo CPU P8600 @2.40 GHz and 4 GB RAM, and the algorithm is currently implemented in *MATLAB*. The computation time shown in this test is used only for comparison purposes and can actually be further improved on other platforms. For the original dynamic optimization algorithm, the computation time refers to directly applying the algorithm on the raw range image. For the proposed algorithm, the computation time includes profile rectification, rough segmentation, and precise segmentation, which are all presented in the experimental results.

Table 1 shows the experimental results. A total of 25 pavement images were tested: 5 images for each crack type (longitudinal, transverse, block, and alligator cracking), and 5 images that were distress-free. The accuracy and computation time are presented for both the original dynamic optimization algorithm and the proposed enhanced algorithm. In addition, Figs. 8–11 show representative pavement images from four crack types and demonstrate the algorithm's performance.

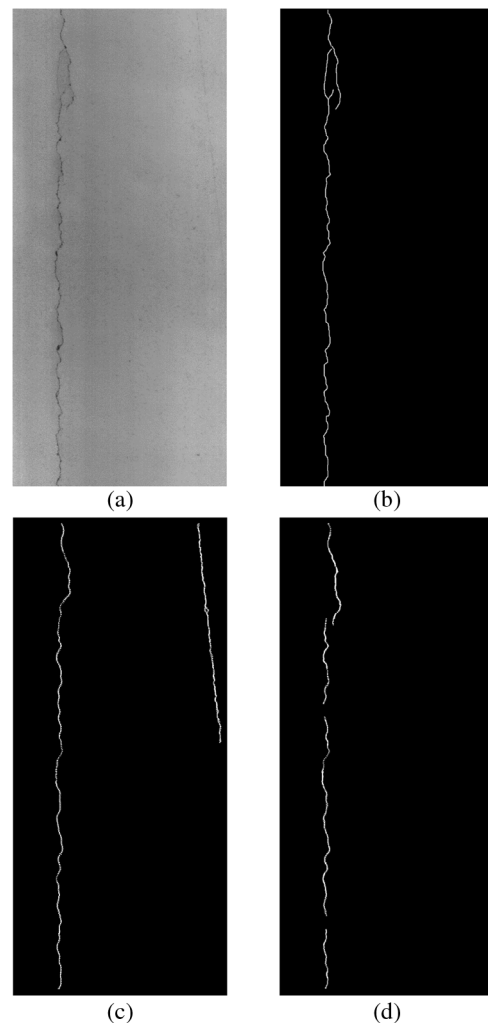


**Fig. 8.** Comparison between the original algorithm and the proposed enhanced algorithm on longitudinal cracking (image no. 1): (a) raw range image; (b) crack segmentation ground truth; (c) crack segmentation using the original dynamic optimization algorithm; (d) crack segmentation using the proposed algorithm

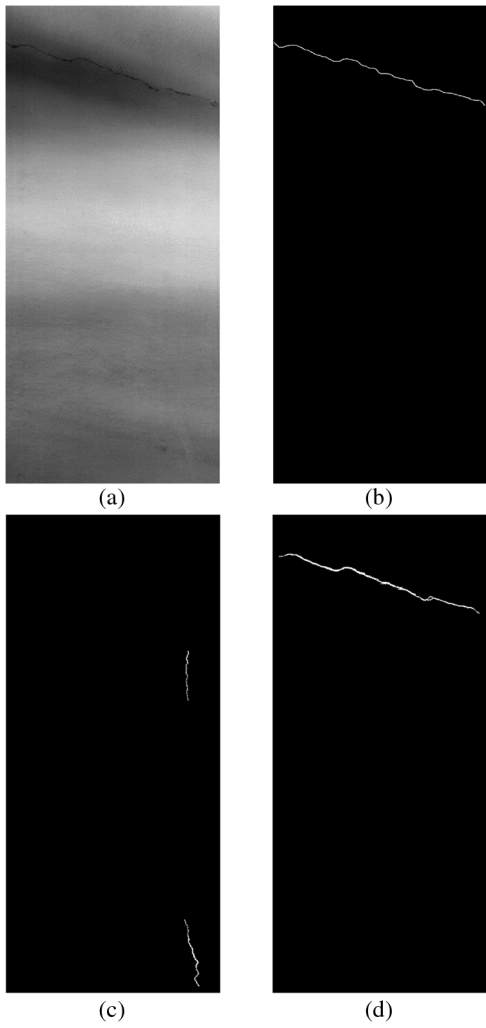


**Fig. 9.** Comparison between the original algorithm and the proposed enhanced algorithm on transverse cracking (image no. 6): (a) raw range image; (b) crack segmentation ground truth; (c) crack segmentation using the original dynamic optimization algorithm; (d) crack segmentation using the proposed algorithm

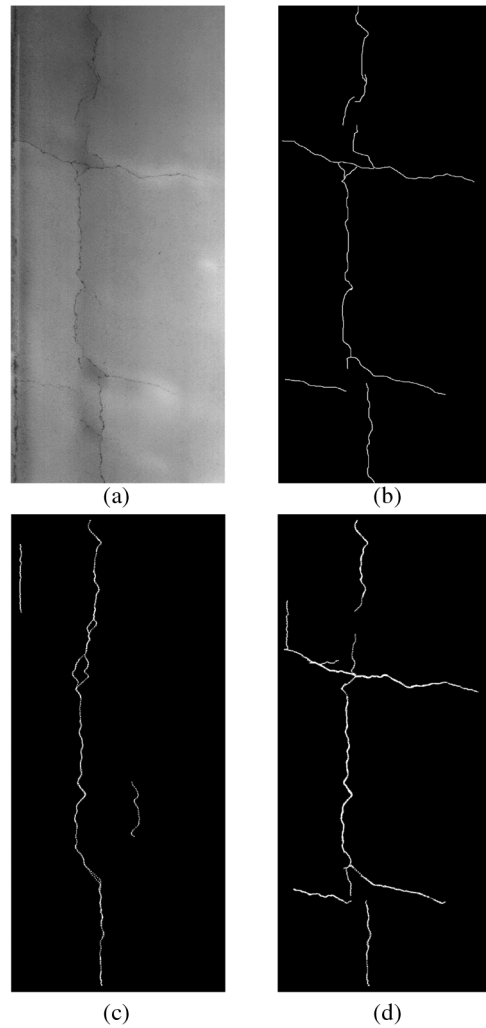


**Fig. 10.** Comparison between the original algorithm and the proposed enhanced algorithm on block cracking (image no. 11): (a) raw range image; (b) crack segmentation ground truth; (c) crack segmentation using the original dynamic optimization algorithm; (d) crack segmentation using the proposed algorithm

Overall, the average computation time was significantly reduced from 122 to 34 s using the proposed algorithm for all 25 selected pavement images. From the perspective of segmentation accuracy, based on the scoring results provided by the buffered Hausdorff distance method, the average segmentation accuracy improved from 57.13 to 88.62 because the proposed algorithm removed unnecessary false positives through the rough segmentation stage and better handled the situation with cracks with multiple orientations. The experimental results show that the proposed method improves the performance of crack segmentation in terms of both accuracy and time consumption.

For simple longitudinal cracking (as shown in Fig. 8), the proposed algorithm located the crack ROIs through the rough segmentation stage, which not only minimized the searching space for dynamic optimization to reduce the time consumption, but also eliminated potential false positives, improving accuracy. For simple transverse cracking (as shown in Fig. 9), the original algorithm cannot perform well because it is orientation sensitive and the default searching direction is set to be longitudinal. It resulted in search iterations with a long processing time, the algorithm was not able to retrieve an optimal crack path, and that led to some false

positives. The proposed algorithm automatically determined the searching direction for each ROI at the rough segmentation stage to maximize the probability of correct segmentation. Similarly, for block cracking (as shown in Fig. 10), the original algorithm still captured the cracks along only one general orientation, and the proposed algorithm clearly segmented cracks on different orientations.

For alligator cracking (as shown in Fig. 11), the computation time using the proposed algorithm is longer than the other three crack types. It can be observed that under the same data format, the time consumption for the first and second stages of the proposed algorithm remained stable, while the computation time of the last stage depended on the detailed crack characteristics of different pavement images. For pavement images with complex crack patterns, more crack ROIs will be identified through the rough segmentation stage, and the precise segmentation will cost more time. As shown in Fig. 11(a), the alligator cracking has spread to the entire image; although being reduced by the proposed algorithm, the remaining search space still covers almost the entire image, which leads to greater time consumption. However, the proposed algorithm still reduces almost half the original computation time

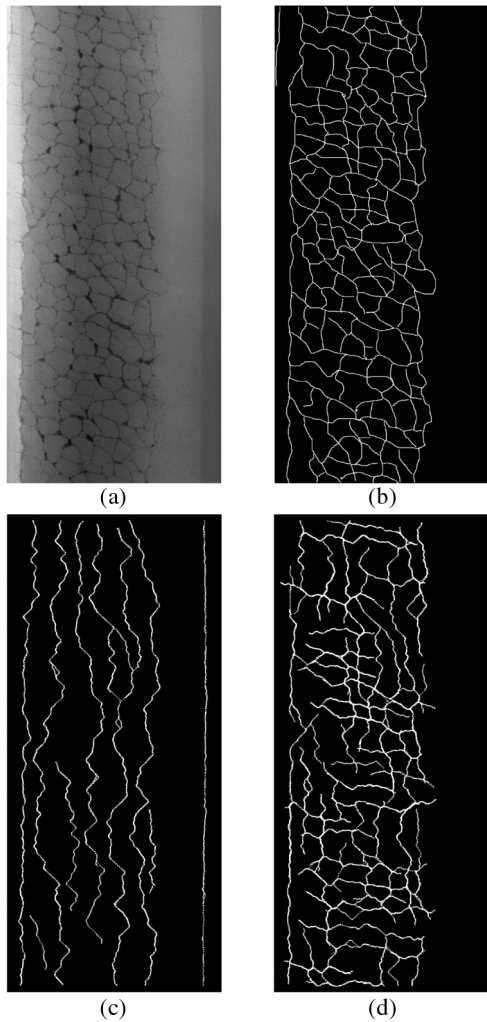


**Fig. 11.** Comparison between the original algorithm and the proposed enhanced algorithm on alligator cracking (image no. 16): (a) raw range image; (b) crack segmentation ground truth; (c) crack segmentation using the original dynamic optimization algorithm; (d) crack segmentation using the proposed algorithm

and clearly improves the segmentation accuracy for all alligator-cracking detection.

In addition, the proposed algorithm performs more robustly on distress-free images. As it reduces almost half the computation time, the accuracy of the proposed algorithm is consistent on all five images in the last category, while the original dynamic optimization algorithm detects false positives in one of the images.

## Conclusions and Recommendations

Developing an automatic pavement crack survey method has attracted much attention from researchers and transportation agencies over the past two decades. Significant efforts have been made on automatic pavement crack segmentation as an essential step before crack classification and evaluation takes place. However, the performance of most existing image-based crack segmentation algorithms remains a challenge, and they are also vulnerable and not robust enough to handle different pavements and lighting conditions. With the advances of sensing technology, a high-resolution 3D line laser imaging system is now available. In 3D pavement

data, pavement cracking becomes more distinctive, with its apparent elevation changes, and the influences of most noises in 2D intensity images have been reduced. A dynamic optimization algorithm, which has been proved in a previous study to have a better performance than other crack segmentation methods, can also be used on 3D pavement data in the format of range images. However, with high data resolution, the computation time of a dynamic optimization algorithm increases exponentially, and the requirement of the searching direction also limits its implementation and performance in real applications.

This study is motivated by the need to take advantage of 3D pavement data on crack segmentation and to develop a robust algorithm in terms of both accuracy and computation time. An enhanced dynamic optimization-based crack segmentation algorithm using 3D pavement data is described in this paper.

The proposed algorithm consists of three major stages. First, a two-step Gaussian filter is applied to remove the outliers from the collected laser data and rectify the profile to reduce the influence of cross-slope and ruts on crack segmentation. Then, a rough crack segmentation stage is conducted to adaptively identify the crack regions of interest. Based on the rectified pavement range image, local thresholding is used to find the initial cracklike pixels, and connected component analysis is then applied to further refine and reduce crack ROIs. Finally, for each valid crack ROI, its bounding box and major orientation provide the necessary searching space and direction for the final precise crack segmentation using the dynamic optimization algorithm. By reducing the size of the search space, the time consumption of the proposed algorithm is significantly reduced, as compared to directly applying the original dynamic optimization algorithm to the entire image. Unlike previous grid-based (image-tile-based) approaches, through fast rough crack segmentation, the selection of crack ROIs is adaptive to the characteristics of pavement distresses. In addition, with the searching direction in each crack ROI, the segmentation accuracy of the proposed algorithm is improved.

Experimental tests were conducted using actual 3D pavement data collected on U.S. 80/Louisville Road near Savannah, Georgia. In order to prove the robustness of the proposed algorithm, the data set was selected to include four different common crack types. A buffered Hausdorff distance-based scoring method was used to quantitatively evaluate the segmentation accuracy of the proposed algorithm, and the computation time was also recorded and compared. Experimental results show that the proposed method has the ability to conduct fast and accurate crack segmentation on 3D pavement data.

The following are recommendations for future research:

- The computation time has been significantly reduced by using the proposed algorithm; however, the current method still may not be able to handle tasks such as large-scale automatic crack surveys. The application of parallel processing can be incorporated in order to further speed up the crack segmentation.
- Although 3D pavement data overcomes the influences of different lighting, shadow, oil stain, and other elements, it is difficult to handle situations with sealed cracks or foreign objects in the cracks (e.g., sands). Therefore, it will be promising to develop a crack segmentation algorithm incorporating both 2D and 3D pavement data.

## Acknowledgments

The work described in this paper was sponsored by the U.S. DOT RITA program (DTOS59-10-H-0003) and the Georgia DOT. The views, opinions, findings, and conclusions reflected in this

presentation are the responsibility of the authors only and do not represent the official policy or position of the U.S. DOT, RITA, Georgia DOT, or any state or other entity. Also, special thanks to Dr. Oleksandr Alekseychuk for allowing us to use the original program of dynamic optimization algorithm for testing.

## References

- Adu-Gyamfi, Y., Okine, N., Garateguy, G., Carrillo, R., and Arce, G. (2012). "Multiresolution information mining for pavement crack image analysis." *J. Comput. Civ. Eng.*, **10.1061/(ASCE)CP.1943-5487.0000178**, 741–749.
- Ahmed, M. F., and Haas, C. (2010). "Potential of low-cost, close-range photogrammetry toward unified automatic pavement distress surveying." *Transportation Research Board Annual Meeting*, National Research Council, Washington, DC.
- Alekseychuk, O. (2006). "Detection of crack-like indications in digital radiography by global optimisation of a probabilistic estimation function." *BAM-dissertationsreihe*, Berlin.
- Capuruço, R., Tighe, S., Li, N., and Kazmierowski, T. (2006). "Performance evaluation of sensor- and image-based technologies for automated pavement condition surveys." *Transportation Research Record 1968*, Transportation Research Board, Washington, DC, 47–52.
- Cheng, H., Chen, J., Glazier, C., and Hu, Y. (1999). "Novel approach to pavement cracking detection based on fuzzy set theory." *J. Comput. Civ. Eng.*, **10.1061/(ASCE)0887-3801(1999)13:4(270)**, 270–280.
- FHWA (Federal Highway Administration). (2015). "National performance management measures; assessing pavement condition for the National Highway Performance Program and bridge condition for the National Highway Performance Program." *Federal Register*, 80(2), 326–393.
- Goodman, S. N. (2001). "Assessing variability of surface distress surveys in canadian long-term pavement performance program." *Transportation Research Record 1764*, Transportation Research Board, Washington, DC, 112–118.
- Haas, C., and Hendrickson, C. (1990). "Computer-based model of pavement surfaces." *Transportation Research Record 1260*, Transportation Research Board, Washington, DC, 91–98.
- Huang, Y., and Tsai, Y. (2011). "Dynamic programming and connected component analysis for an enhanced pavement distress segmentation algorithm." *Transportation Research Record 2225*, Transportation Research Board, Washington, DC, 89–98.
- Jahanshahi, M., Jazizadeh, F., Masri, S., and Becherik-Gerber, B. (2013). "Unsupervised approach for autonomous pavement-defect detection and quantification using an inexpensive depth sensor." *J. Comput. Civ. Eng.*, **10.1061/(ASCE)CP.1943-5487.0000245**, 743–754.
- Kaul, V., Tsai, Y., and Mersereau, R. (2009). "A quantitative performance evaluation of pavement distress segmentation algorithms." *Transportation Research Record 2153*, Transportation Research Board, Washington, DC, 106–113.
- Laurent, J., Lefebvre, D., and Samson, E. (2008). "Development of a new 3D transverse laser profiling system for the automatic measurement of road cracks." *6th Symp. Pavement Surface Characteristics—SURF*, World Road Association (PIARC), La Défense Cedex, France.
- Lee, B., and Lee, H. (2004). "Position-invariant neural network for digital pavement crack analysis." *Comput.-Aided Civ. Infrastruct. Eng.*, **19**(2), 105–118.
- MATLAB 2015a [Computer software]. Natick, MA, MathWorks.
- Mraz, A., Amarasingi, S., Gunaratne, M., and Nazef, A. (2007). "Innovative method for enhancing pavement crack images." *Transportation Research Board Annual Meeting*, Transportation Research Board of the National Academies, Washington, DC.
- Mraz, A., Gunaratne, M., Nazef, A., and Choubane, B. (2006). "Experimental evaluation of a pavement imaging system: Florida Department of Transportation's multipurpose survey vehicle." *Transportation Research Record 1974*, Transportation Research Board, Washington, DC, 97–106.
- Tighe, S., Li, N., and Kazmierowski, T. (2008). "Evaluation of semiautomated and automated pavement distress collection for network-level pavement management." *Transportation Research Record 2084*, Transportation Research Board, Washington, DC, 11–17.
- Tsai, J., Kaul, V., and Mersereau, R. (2010). "Critical assessment of pavement distress segmentation methods." *J. Transp. Eng.*, **10.1061/(ASCE)TE.1943-5436.0000051**, 11–19.
- Tsai, Y., Jiang, C., and Huang, Y. (2014). "Multiscale crack fundamental element model for real-world pavement crack classification." *J. Comput. Civ. Eng.*, **10.1061/(ASCE)CP.1943-5487.0000271**, 04014012.
- Wang, K. C. P. (2000). "Designs and implementations of automated systems for pavement surface distress survey." *J. Infrastruct. Syst.*, **10.1061/(ASCE)1076-0342(2000)6:1(24)**, 24–32.
- Wang, K. C. P., and Gong, W. (2002). "Real-time automated survey of pavement surface distress." *7th Int. Conf. on Applications of Advanced Technologies in Transportation*, ASCE, Reston, VA, 465–472.
- Xu, B. (2005). "Artificial lighting for the automated pavement distress rating system." Univ. of Texas at Austin, Austin, TX.
- Xu, B. (2007). "Summary of implementation of an artificial lighting system for automated visual distress rating system." *Transportation Research Board Annual Meeting*, Transportation Research Board of the National Academies, Washington, DC.
- Zhou, J., Huang, P., and Chiang, F.-P. (2005). "Wavelet-based pavement distress classification." *Transportation Research Record 1940*, Transportation Research Board, Washington, DC, 89–98.
- Zhou, J., Huang, P., and Chiang, F.-P. (2006). "Wavelet-based pavement distress detection and evaluation." *Opt. Eng.*, **45**(2), 027007.
- Zou, Q., Cao, Y., Li, Q., Mao, Q., and Wang, S. (2012). "CrackTree: Automatic crack detection from pavement images." *Pattern Recognition Letters*, **33**(3), 227–238.